frontiers in Marine Science

ORIGINAL RESEARCH
published: 30 July 2021
doi: 10.3389/fmars.2021.692631

Novel Application of ^{210}Po-^{210}Pb Disequilibria to Date Snow, Melt Pond, Ice Core, and Ice-Rafted Sediments in the Arctic Ocean

Mark Baskaran and Katherine Krupp*

Department of Environmental Science and Geology, Wayne State University, Detroit, MI, United States

We collected surface ocean water, snow, grab ice, ice core, melt pond and ice-rafted sediment (IRS) from 5 ice stations during the Western Arctic US GEOTRACES cruise (USGCG Healy; August 10 – October 7, 2015) and analyzed for ^{210}Po ($T_{1/2}$ = 138.4 days) and ^{210}Pb ($T_{1/2}$ = 22.3 years) in dissolved and particulate phases (snow, grab ice, ice core, surface seawater) to investigate the ^{210}Po:^{210}Pb disequilibria in these matrices. Thirteen aerosol samples, using a large-volume aerosol sampler (PM10), from Dutch Harbor, AK to North Pole, were also collected and analyzed for ^{210}Po/^{210}Pb to quantify the atmospheric depositional input to the snow and surface waters. Falling snowfall is tagged with ^{210}Po/^{210}Pb ratio (AR) similar to that in the air column from the cloud condensation height to air-sea interface. From the measured AR in aerosol and snow, modeling the sources of ^{210}Po and ^{210}Pb input to the melt pond, and measured disequilibrium in ice core and ice-rafted sediment, we show ^{210}Po/^{210}Pb AR is a novel chronometer to date snow, ice core, melt pond, and IRS. The calculated mean ages of aerosol, snow, melt pond and IRS are 12 ± 7 (n = 13), 13 ± 11 (n = 6), 60 ± 14 (n = 4), and 87 ± 23 (n = 6) days, respectively. The average IRS age corresponds to an average drift velocity of sediment-laden ice of 0.18 ± 0.06 (n = 6) m s^{-1}. We report highly elevated levels of ^{210}Po and ^{210}Pb in snow and melt pond compared to those in Arctic surface seawater and enrichment of ^{210}Po compared to ^{210}Pb onto particles extracted from snow, ice and melt ponds. The observed disequilibrium between ^{210}Po and ^{210}Pb in ice could serve as a quantitative tool in delineating multiple-year ice from seasonal ice as well as a metric in quantifying the speed of ice/snow melting and delay in autumn freeze.

Keywords: Po-210/Pb-210 dating, Arctic pollutant transport, dating ice-rafted sediment, dating of snow and melt pond, Po-210 enrichment in particulate matter, environmental changes in the Arctic

OPEN ACCESS

Edited by:
Laodong Guo,
University of Wisconsin–Milwaukee, United States

Reviewed by:
Guebuem Kim,
Seoul National University, South Korea
Xilong Wang,
Beibu Gulf University, China

****Correspondence:***
Mark Baskaran
Baskaran@wayne.edu
orcid.org/0000-0002-2218-4328

Specialty section:
This article was submitted to Marine Biogeochemistry, a section of the journal Frontiers in Marine Science

Received: *08 April 2021*
Accepted: *18 June 2021*
Published: *30 July 2021*

Citation:
Baskaran M and Krupp K (2021) Novel Application of ^{210}Po-^{210}Pb Disequilibria to Date Snow, Melt Pond, Ice Core, and Ice-Rafted Sediments in the Arctic Ocean. Front. Mar. Sci. 8:692631. doi: 10.3389/fmars.2021.692631

INTRODUCTION

The Arctic is undergoing drastic environmental change which has manifested in decrease in the areal extent of sea ice cover, from 6.95 million km^2 in 1980 to 3.95 million km^2 in 2015, ∼45% decrease which is attributed to increase in sea surface as well as surface air temperature. Earlier melt of sea ice and later freeze in the Arctic shelves lead to a longer open-water season which has

impacted the biogeochemical cycling of key trace elements and isotopes due to wind-driven vertical mixing (Kipp et al., 2018; Rutgers van der Loeff et al., 2018; Grenier et al., 2019). In addition, early retreat of sea ice edge is expected to result in higher wave action which in turn, expected to affect the amount of energy transferred from wind to surface water. Ice-free shelf waters are anticipated to result in higher wind-driven upwelling which in turn is expected to increase the amount of deeper waters onto the shelf (Carmack and Chapman, 2003). Thus, the residence time of snow, ice, and melt ponds is of great interest and has bearing on the changes in the biogeochemical cycling. The age of snow, melt pond, ice and ice-rafted sediment (IRS) in the Arctic Ocean has direct relevance to the total heat energy absorbed by surface water due to differences in their albedo and heat transfer during phase change (e.g., heat absorbed by snow/ice to become liquid water) (Uttal et al., 2002).

Polonium-210 (^{210}Po, $T_{1/2}$ = 138.4 days) and lead-210 (^{210}Pb, $T_{1/2}$ = 22.3 years), progeny of radon-222 [^{222}Rn, half-life ($T_{1/2}$) = 3.82 days], the heaviest and longest-lived noble gas in the U-Th series, are particle-reactive and thus have been utilized as tracers and chronometers in environmental studies (Robbins, 1978; Turekian et al., 1977; Cochran and Masque, 2003; Rutgers van der Loeff and Geibert, 2008; Baskaran, 2016). A major fraction of ^{210}Pb in surface ocean waters is derived from direct atmospheric deposition, which is derived from the decay of atmospheric Radon (e.g., Bacon et al., 1976). A small fraction of ^{222}Rn, daughter of ^{226}Ra, produced in rocks and mineral grains on the Earth's upper crust escapes through cracks and crevices to the atmosphere. From there, it embarks on its journey in the atmosphere via advection and diffusion and produces 12 different isotopes, including ^{210}Po and ^{210}Pb (Turekian et al., 1977). The radon emanation rates from continents decrease with increasing latitude by a factor of 5, from 1 atom cm^{-2} s^{-1} at 30°N to 0.2 atom cm^{-2} s^{-1} at 70°N (Conan and Robertson, 2002; Baskaran, 2011). In addition, the average ^{222}Rn emanation rate from the continental area (including land area covered by glaciers and permafrost with negligible ^{222}Rn release) of 0.75 atom cm^{-2} s^{-1} is ∼1-2 orders of magnitude higher compared to surface waters (rivers, lakes, and ocean) (e.g., Wilkening and Clements, 1975). In the absence of ^{210}Po from sources other than the radioactive decay of atmospheric ^{222}Rn-derived ^{210}Pb (such as volcanic, industrial release, etc.), the ^{210}Po/^{210}Pb activity ratio (AR) in aerosols has been utilized to determine the 'age' of aerosols (Moore et al., 1973; Robbins, 1978; Marley et al., 2000) and is generally reported to be <0.1 in the lower and middle troposphere (Turekian et al., 1977; Baskaran, 2011).

The upper end of the dating range of a radioactive daughter-parent pair, where the parent half-life is much longer than the daughter half-life, is typically about 5-6 half-lives of the daughter isotope and hence ^{210}Po:^{210}Pb disequilibrium is useful from a few days up to 2 years. From simultaneous measurements of ^{210}Po and ^{210}Pb in aerosols and precipitation, it was shown that the initial ^{210}Po/^{210}Pb AR was similar in rain/snow and aerosols (McNeary and Baskaran, 2007). During precipitation in the Arctic (and elsewhere), the falling snow underneath the cloud cover is tagged with the ^{210}Po/^{210}Pb AR of aerosols generally with values of <0.1 (Baskaran, 2011); as time elapses, this ratio in snow increases due to ^{210}Po ingrowth from the decay of ^{210}Pb. With time, the accumulated snow becomes ice or undergoes melting. During the beginning of the melt season, generally in June, meltwater from snow and ice, mostly freshwater, begins to form a pond at the surface and grow, both in areal extent and depth (Polashenski et al., 2012). From the estimated initial and measured ^{210}Po/^{210}Pb AR of the melt pond, its age can be determined. During storm events in early autumn, atmospherically delivered ^{210}Po and ^{210}Pb, with ^{210}Po/^{210}Pb AR of <0.1, are scavenged by resuspended sediments and eventually incorporated into coastal sea ice which are subsequently transported to the interior Arctic (Nürnberg et al., 1994). The in-growth of ^{210}Po from the decay of ^{210}Pb provides the time elapsed since incorporation of these radionuclides. Here, we report a novel application of disequilibrium between ^{210}Po and ^{210}Pb in dating snow, melt pond, ice core and IRS collected from the Arctic Ocean.

The primary goal of the present study, is to test the following hypotheses: (i) The in-growth of ^{210}Po from the decay of ^{210}Pb in snowfall provides a tool to determine the age of snow; (ii) From quantifying the fractional input of the sources of water to the melt pond and knowing the end-member activities of ^{210}Po and ^{210}Pb, the age of the melt ponds can be determined; (iii) Since the time range for daughter-deficient ^{210}Po:^{210}Pb dating is up to ∼ 2 years (or ^{210}Po/^{210}Pb ∼0.97), multi-year ice in ice-pack can be recognized; and (iv) Most of the atmospherically delivered ^{210}Pb, with ^{210}Po/^{210}Pb AR similar to that in aerosol, is scavenged by resuspended sediment which gets incorporated into sea ice in the coastal areas and thus, we can date the IRS using ^{210}Po/^{210}Pb pair. The ages of snow, melt pond and ice core are relevant to the exchange of latent heat with the surrounding, changes in the albedo while ages of IRS are relevant to the transport velocity of coastal sediments and sediment-laden contaminants. In addition, transport of nutrients from coastal zone to the deep Arctic through sea ice makes a coupling between coastal and deep arctic benthic community.

MATERIALS AND METHODS

Sample Collection

During US GEOTRACES Arctic cruise (HLY1502; R/V Icebreaker USCGC *Healy;* August 10 – October 7, 2015), the following samples were collected from 6 ice stations (ST-31, -33, -39, -42, -43, and -46, **Figure 1**): snow, melt pond (only 5 stations) and ice core; IRS, often are sporadically distributed in the ice, from two ice stations (E-6195 and -6244); and 13 aerosol samples (**Figure 1**), using a large-volume aerosol sampler (PM_{10}), from Dutch Harbor, AK to North Pole, where each deployment averaged ∼30 h of run time (**Figure 1** and **Table 1**). Aliquots of GFF aerosol filters, corresponding to filtered air volume, 72 to 463 m^3 (**Table 1**), were provided for analysis from the aerosol group of the U.S. GEOTRACES program. Details on aerosol collection were published in Morton et al. (2013).

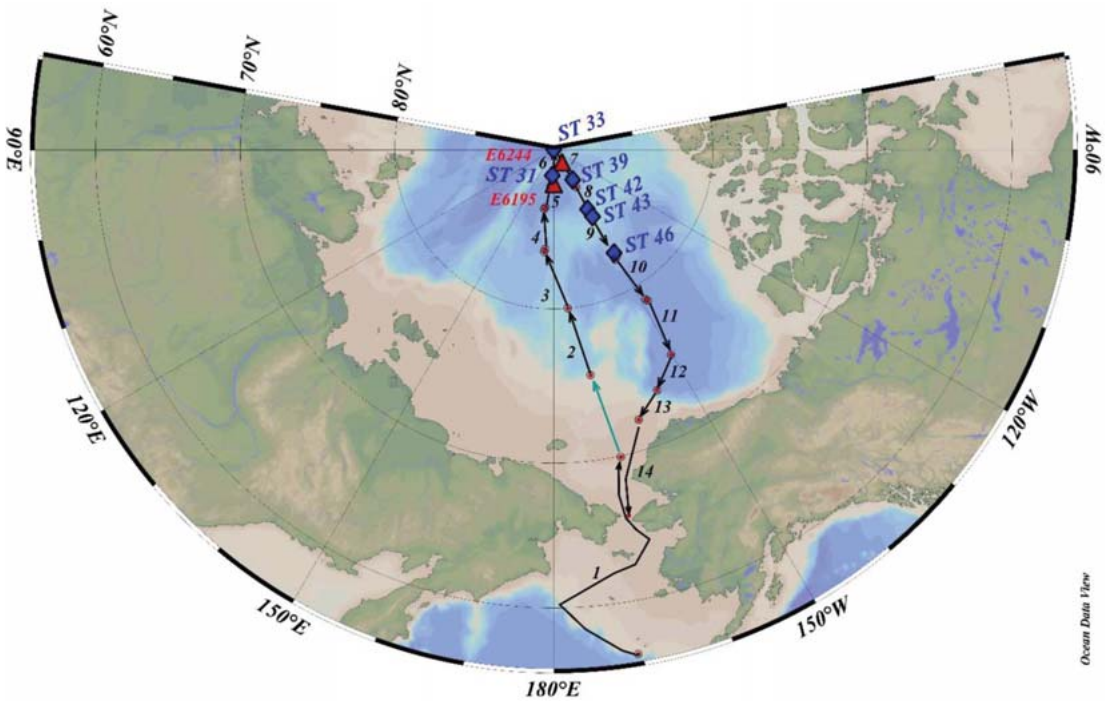

FIGURE 1 | Sampling stations for aerosols, ice-rafted sediment and ice stations. Green arrow shows transit with no sampling; distance between successive red dots denote aerosol sampling (starting and ending of location) for that particular sample; pumps didn't work for ST-5 and no sample. Two red lettered stations (E6244 and E6195 in red triangle) denote the dirty sea ice sample collection; Blue lettered stations 31, 33, 39, 42, 43, and 46 denote ice stations (US GEOTRACES Arctic cruise, HLY1502, R/V Icebreaker USCGC *Healy*).

Appropriate care was taken in preventing plume discharged from the ship's chimney when sailing. Since a large number of trace metals were also analyzed in the same aerosol filters, extreme caution was exercised in sample collection. At ice stations, bulk snow deposited on sea ice were collected into precleaned plastic bags and melted onboard to a volume of 20 L and filtered. For melt pond water samples, a hole was drilled in the frozen closed melt ponds using a TM-clean corer. A battery-powered peristaltic pump with silicone tube was used to fill a carboy with unfiltered water (Kadko and Landing, 2015; depth of the melt pond not known) and was filtered onboard. In each of the 6 ice stations, 2 ice cores next to each other, from surface to all the way down to the seawater, were collected with the Kovaks corer (9 cm ID), evenly divided into 5-6 segments approximately 20-40 cm each and same segments were combined, and melted in the onboard laboratory. The melt water from snow, ice core, and melt pond water were filtered using 0.4 μm Whatman Nuclepore track-etched membrane filter in a vacuum filtration system and the material retained in the filter were considered particulate matter. All filters were retained for particulate analysis, and filtered water samples were acidified to a pH of 2 with 6M HCl and the preconcentration was done following $Fe(OH)_3$ method (details in Methodology). The IRS was collected by shoveling sediment-laden ice (sediment found both at the surface and inside of the ice fragments), into pre-cleaned 20 L buckets, melted, sediments were allowed to settle, and the 'supernatant' meltwater was poured off to concentrate the sample. The sediment solution was then dried in an oven at 100°C and used for further analysis.

Development of Chemical Leaching Method for Aerosol Filter and Ice-Rafted Sediment for ^{210}Po and ^{210}Pb

The general procedure for measuring ^{210}Po and ^{210}Pb in aerosol and involves complete digestion using concentrated hydrochloric acid, nitric acid, and hydrofluoric acid, followed by drying, and then taken in dilute HCl solution for electroplating. Since the *in situ* ^{210}Po/^{210}Pb AR in aerosol is generally less than 0.1 (Baskaran, 2011), it is a prerequisite that *in situ* ^{210}Po is separated from *in situ* ^{210}Pb soon after the sample collection (note: in 30 days from sample collection to Po plating, 14% in-growth ^{210}Po would take place). In order to avoid usage of concentrated hydrofluoric acid on the ship, prior to the cruise we tested a series of different leaching procedures in one aerosol filter (aerosol sample collected at Wayne State University campus, Detroit, MI, United States) by both leaching and total digestion, and compared the amount of ^{210}Po extracted by each method performed on separate aliquots of the same filter. The aerosol sample was filtered through one 8″ × 10″ QFF filter at a flow rate of 1.4 m^3/min for approximately 24 h, similar to the arctic aerosol samples collection (**Table 1**). The filter was cut into 4 quarters and were weighed. Visual observation of the filter and the weights indicated uniform aerosol mass distribution. The

TABLE 1 | Aerosol collection time, location, volume, activities and depositional fluxes of ^{210}Po and ^{210}Pb and ^{210}Po/^{210}Pb AR.

#: Event, Deployment	Start-end Date	Latitude (N)	Longitude (W)	Volume	^{210}Po	^{210}Pb	^{210}Po/^{210}Pb	^{210}Po flux	^{210}Pb flux
	[dd/mm/yyyy]	Start-End	Start-End	m^3	dpm/100 m^3	dpm/100 m^3	AR	dpm cm^{-2} y^{-1}	dpm cm^{-2} y^{-1}
6060-1	10-17/8/2015	56.074-69.926	170.509 to 167.688	463	0.0042 ± 0.0003	0.056 ± 0.003	0.074 ± 0.007	0.0013 ± 0.0001	0.018 ± 0.001
6123-2	20-23/8/2015	75.566-79.997	170.75-174.953	174	0.023 ± 0.001	0.42 ± 0.01	0.054 ± 0.004	0.0071 ± 0.0004	0.133 ± 0.004
6149-3	23-27/8/2015	80.001-83.572	174.96 to −174.731	275	0.033 ± 0.002	0.63 ± 0.03	0.052 ± 0.004	0.0103 ± 0.0006	0.20 ± 0.01
6168-4	27-30/8/2015	83.757-86.244	−175.043 to −170.654	118	0.049 ± 0.004	0.64 ± 0.02	0.077 ± 0.007	0.0156 ± 0.0012	0.20 ± 0.01
6236-6	4-8/9/2015	88.408-89.945	−176.752 to 97.848	272	0.029 ± 0.002	0.63 ± 0.02	0.046 ± 0.004	0.0090 ± 0.0006	0.20 ± 0.01
6267-7	8-12/9/2015	89.941-87.352	104.19 to 149.43	116	0.012 ± 0.001	0.63 ± 0.02	0.019 ± 0.002	0.0037 ± 0.0003	0.20 ± 0.01
6304-8	12-16/9/2015	87.2785.145	149.044 to 149.855	72	0.0010 ± 0.0001	0.34 ± 0.02	0.0030 ± 0.0003	0.0003 ± 0.0000	0.11 ± 0.01
6347-9	17-20/09/2015	85.163-82.259	150.395 to 149.377	108	0.00039 ± 0.0003	0.43 ± 0.02	0.0090 ± 0.0009	0.0012 ± 0.0001	0.14 ± 0.01
6387-10	21-26/09/2015	82.101-78.974	150.811 to 148.501	320	0.0085 ± 0.0006	0.60 ± 0.02	0.014 ± 0.001	0.0027 ± 0.0002	O.lfttO.01
6424-11	26-29/09/2015	78.804-75.047	148.093 to 150.176	116	0.035 ± 0.003	2.15 ± 0.18	0.016 ± 0.001	0.0110 ± 0.0008	0.68 ± 0.03
6444-12	29/09-3/10/2015	75.06-73.426	150.215 to 156.793	211	0.028 ± 0.002	0.75 ± 0.03	0.037 ± 0.003	0.0088 ± 0.0006	0.24 ± 0.01
6487-13	3-7/10/2015	73.397-71.998	156.766 to 162.562	151	0.031 ± 0.002	0.95 ± 0.04	0.033 ± 0.003	0.0098 ± 0.0007	0.30 ± 0.01
6495-14	7-9/10/2015	72.004-65.95	162.56 to 168.449	90	0.055 ± 0.004	0.76 ± 0.05	0.073 ± 0.007	0.0175 ± 0.0011	0.24 ± 0.02
						Average:	0.039 ± 0.026	0.0076 ± 0.005	0.22 ± 0.15

aerosol collection occurred from May 23 to May 24, 2015 and ^{210}Po plating was performed on the same day of retrieval. To each aliquot, varying concentrations of hydrochloric and nitric acid were used (**Table 2**). For leaching, an aliquot of the filter along with the acids (**Table 2**) was taken in a centrifuge tube and placed in an ultrasonic bath at 70°C. The filtrate was then separated from filter by vacuum filtration and the process was repeated once more. The solutions were combined and processed further for ^{210}Po plating (Krupp, 2017). The typical time involved are: leaching (2 h total), digestion (12 h), and drying (∼6-8 h). Additional details are given in Krupp (2017).

The calculated ^{210}Po activities are given in **Table 2**. We report that leaching of the filter with 6M hydrochloric acid + 8M nitric acid, followed by drying (necessary to prevent dissolution of planchet in nitric acid medium) and dilution, provided results consistent with total digestion with HF (^{210}Po = 0.329 ± 0.013 dpm 100 m^{-3} vs. 0.315 ± 0.013 dpm 100 m^{-3} for leaching and HF digestion, respectively). The results show that 6M hydrochloric acid leaching alone is not sufficient (^{210}Po = 0.250 ± 0.009 dpm 100 m^{-3}), suggesting that nitric acid is necessary as an oxidizing agent to quantitatively extract ^{210}Po from the aerosol filter due to possible presence of ^{210}Po-laden organic aerosol particles. These results also suggest that the complete destruction of the quartz fiber by hydrofluoric acid is not necessary to extract ^{210}Po from the filter media, implying that sorbed ^{210}Po onto lithogenic particles can be quantitatively removed by a mixture of 6M HCl + 8M HNO_3 alone. This leaching method was used in place of total digestion on the cruise in order to eliminate the need for hydrofluoric acid and concentrated nitric and hydrochloric acid, as well as reduce the time usually needed to digest the aerosol filters, which is important when considering the time-sensitivity of the ^{210}Po isotope and the volume of work involved onboard the ship.

In most of the enriched ^{210}Po and ^{210}Pb are sorbed onto sediment surface, we tested a set of leaching methods. Approximately 12 L of dirty lake ice using a 20 L plastic bucket was collected on March 14-15, 2015 near the mouth of the Clinton River which discharges into Lake St. Clair in southeast Michigan. After melting (melt volume = 8.7 L), settling (after 48 h), decanting, and drying the concentrated solution in an oven (48-72 h), the total amount of dried silty-clay sediment collected was 3.617 g. To ensure fine clays were collected, the decanted ice solution was subsequently allowed to settle (48 h) and then dried in the same manner, providing a total amount of clay sediment of 0.242 g. This was combined with the other aliquot of 3.617 g. The collected sediments overall were fine-textured and grayish-brown, and included a small amount of macro-organic material (grass and hairs) which was removed before leaching. About 0.2 g of the homogenized sediment sample was leached for 1 h at ∼90°C with 10 mL of 6M HCl twice and the leachate were combined. The combined solution was dried and taken in 5 mL 1 M HCl and gamma counted. To minimize time, acid consumption and waste generation onboard, results from a leaching experiment showed that 6M HCl leaching of

TABLE 2 | Activities for aerosol filter aliquots processed by total digestion or two leaching methods.

Method	^{210}Po (dpm/100 m^3 air)
Digestion (10 mL of HCl, HNO_3, HF, dry and dilute)	0.315 ± 0.013
Leaching (10 mL of 6M HCl, 10 mL of 8M HNO_3, dry and dilute)	0.329 ± 0.013
Leaching (20 mL of 6M HCl dilute only)	0.250 ± 0.009

ice-rafted sediment collected from Lake St. Clair quantitatively extracts ^{210}Po and ^{210}Pb from IRS (Krupp, 2017).

Analytical Procedure for ^{210}Po and ^{210}Pb

Polonium-210 and ^{210}Pb activities of snow, ice, melt pond, seawater and aerosol were measured on the same sample. IRS samples were divided into two fractions, one for gamma spectrometry to measure ^{210}Pb and the other for ^{210}Po by alpha spectrometer. Precise determination of *in situ* ^{210}Po requires that the sample be analyzed soon after the collection to minimize in-growth of ^{210}Po. The dissolved phase (filtrate of melt water of snow, ice core and melt pond) was acidified with 5 ml/L of 6M HCl (Trace-Metal grade) to prevent the loss of ^{210}Po and ^{210}Pb by sorption on to the container wall. Each acidified sample was spiked with: (i) a known amount of ^{209}Po US-NIST Standard Reference Material as an internal yield tracer; (ii) 20 mg stable lead via a stable lead carrier of $PbCl_2$ in order to determine chemical efficiency of ^{210}Pb recovery; and (iii) iron carrier ($FeCl_3$; 5 mg Fe/L of water) to co-precipitate ^{210}Po and ^{210}Pb with $Fe(OH)_3$ precipitate. After 12-24 h equilibration period and periodic vigorous shaking of the sample, ammonium hydroxide was added to samples to increase the pH from 2 to 4, and then, 1 mL of 10% sodium chromate was added to samples to increase the lead yield by the co-precipitation of lead chromate. Then, the pH was increased to ∼8. This rise in pH causes the iron to flocculate to co-precipitate ^{210}Po and ^{210}Pb with $Fe(OH)_3$. Details on separation of precipitate and solution, chemical processing and plating of Po are given in Niedermiller and Baskaran (2019). After Po plating, each solution was transferred to a precleaned 60 ml Nalgene bottle and stored for further onshore ^{210}Pb analysis. After polonium plating, any residual ^{210}Po (and ^{209}Po) must be removed from sample solution for the future measurement of *in situ* ^{210}Pb, which is measured by in-growth of ^{210}Po from the decay of ^{210}Pb. Details on the quantitative removal of ^{210}Po using a column separation technique, chemical efficiency determination for ^{210}Pb are given in Niedermiller and Baskaran (2019). Details on decay and in-growth corrections for ^{210}Po and ^{210}Pb are given in Baskaran et al. (2013), Rigaud et al. (2013), Cookbook (2014).

All particulate samples (from snow, ice, melt pond samples) processing was performed using leaching methods. The particulate sample was taken in a 50-ml centrifuge tube and was leached with 10 mL 6M Omni-trace HCl and 10 mL 8M HNO_3 mixture with agitation for 1 h at 70°C in an ultrasonic bath. Subsequently, the solution was filtered, spiked, with a known amount of ^{209}Po and stable Pb, and dried. To the residue, 2 mL of HCl was added and warmed it to bring the residue to solution and then diluted to 40 ml with deionized water. This solution was used for electroplating.

The ^{210}Po-plated discs were assayed in an Octete PC-8 input alpha spectrometer. The background subtraction in most of the samples was less than 0.1% of the net counts for both ^{210}Po and ^{210}Pb. The activities of ^{210}Pb in IRS samples were measured directly in a high-resolution, high-purity Ge well detector coupled to DSA multi-channel analyzer. The gamma-ray spectrometer was calibrated with RGU-1, RGU-Th, both IAEA Certified Reference Materials, periodically. Details on the chemical procedures, counting methods and reagent blanks subtracted, QA/QC and intercalibration results are given below.

Blanks and QA/QC

We ran a total of 17 blanks (6 blank aerosol filters with reagent blanks, 2 reagent blanks for IRS, and 9 reagent blanks for snow, ice core, and melt ponds) for both ^{210}Po and ^{210}Pb. Due to very low activities of ^{210}Po in aerosols (generally ∼5% as that of ^{210}Pb), the blank levels are relatively high, as expected. The average blank activity accounted for 43-83% (mean: 60%, n = 6) for ^{210}Po and 10.4-60.9% (mean: 28.2%, n = 6) for ^{210}Pb. For snow samples, the reagent blank for particulate ^{210}Po ($^{210}Po_p$) and $^{210}Pb_p$ accounted for 0.2-12.5% (mean: 5.5%), and 0.5-14.0% (mean: 4.3%, n = 6), respectively. The corresponding values for dissolved ^{210}Po ($^{210}Po_d$) and $^{210}Pb_d$ accounted for 0.3-5.3% (mean: 2.0%, n = 6) and 0.2-0.8% (mean: 0.4%, n = 6), respectively. The ^{210}Po blank in ice-rafted sediment varied from 0.3 to 3.2% (mean: 1.1%, n = 6). For melt pond samples, the reagent blank values for particulate $^{210}Po_p$ and $^{210}Pb_p$ are higher due to lower activities, accounting for 16.8-48.7% (mean: 24.8%, n = 5), and 8.8-66.0% (mean: 28.3%, n = 5), respectively. The corresponding values for $^{210}Po_d$ and $^{210}Pb_d$ accounted for 0.6-3.9% (mean: 2.0%, n = 5) and 0.9-9.4% (mean: 3.5%, n = 6), respectively. The melt volume of segment of ice core sample was small with lower ^{210}Po and ^{210}Pb activities compared to snow and hence the reagent blanks are higher, accounting for 2.8-89.7% (mean: 48.9%, n = 31) for $^{210}Po_p$, and 3.5-96.3% (mean: 49.3%, n = 31) for $^{210}Pb_p$ and 2.0-68.9% (mean: 33.3%, n = 31) for $^{210}Po_d$, and 4.9-82.9% (mean: 28.2%, n = 31)$^{210}Pb_d$.

We analyzed Certified Reference Material (CRM) RGU-1 (^{238}U concentration 400 ± 2 ppm, with all the progeny of ^{238}U in secular equilibrium, including ^{210}Pb and ^{210}Po; IAEA CRM) eight different times as blind samples following the same procedure as the samples determined by alpha spectrometry to assess the accuracy. About 30 mg (weighed to a precision of ±0.1 mg) of the standard (∼9 dpm) was taken each time and about 5.5 dpm of ^{209}Po spike was added. The same chemical procedure was followed as was outlined in Baskaran et al. (2013). Agreement between the measured and certified value is excellent. The ratio of measured activity to certified value of RGU-1 varied between 0.96 ± 0.01 and 1.02 ± 0.00, with a mean value of 1.00 ± 0.01.

The intercalibration exercise between Wayne State University and Louisiana State University (LSU) showed that the ^{210}Po and ^{210}Pb activities on four water samples (two from GEOTRACES station in the Arctic and two collected from Gulf of Mexico

collected by Dr. Kanchan Maiti, LSU) agreed within 1 standard deviation from each other and hence our ^{210}Po and ^{210}Pb data are of high quality. The results from the intercalibration was submitted to BCO-DMO data center along with all of our ^{210}Po and ^{210}Pb data obtained during 2015 GEOTRACES cruise.

RESULTS AND DISCUSSION

Residence Time and Depositional Velocity of Aerosol Using ^{210}Po and ^{210}Pb and Their Fluxes

The mean specific activity of ^{210}Po and ^{210}Pb in aerosols, 0.023 ± 0.018 (range: 0.0004-0.055, n = 13) dpm 100 m^{-3} (1 dpm = 1 disintegration per minute = 1 atom decaying per minute; 60 dpm = 1 Bq) and 0.69 ± 0.18 (range: 0.06-2.15, n = 13) dpm 100 m^{-3}, respectively (**Table 1**), are significantly lower than those reported in sub-Arctic latitudes (e.g., ^{210}Po: 0.43 (range: 0.11-0.71, n = 30) dpm 100 m^{-3}; ^{210}Pb: 6.9 range: 1.8-25.3, n = 30) dpm 100 m^{-3} in Detroit, MI, United States (42°25′N, McNeary and Baskaran, 2003). Land-derived air masses have significantly higher ^{210}Pb activity compared to maritime air masses due to differences in the ^{222}Rn emanation rates between ocean surface, 0.102 dpm cm^{-2} day^{-1}, and land surface, 7.8-10.8 dpm cm^{-2} day^{-1} (Baskaran, 2011). Long-term global ^{222}Rn fluxes were found to decrease with increasing latitude, from 0.57 ± 0.38 atom cm^{-2} s^{-1} (n = 46) at 30-40°N latitudinal belt to ≤0.12 ± 0.11 atom cm^{-2} s^{-1} (n = 19) at north of 60-70°N belt (Baskaran, 2011). An order of magnitude variations in ^{210}Pb activities is mainly attributed to variations in sources of air masses. Since samples were collected during transit covering large distances (**Figure 1** and **Table 1**), it is not possible to quantitatively assess the influence of land-derived vs. maritime air masses.

The calculated depositional flux of ^{210}Po or ^{210}Pb ($F_{Po\ or\ Pb}$), using eq. (1), from the measured activity of ^{210}Po (C_{Po}) or ^{210}Pb (C_{Pb}) (**Table 1**), assuming aerosol deposition velocity (V_d) of 1 cm s^{-1} (average of 8 global sites, McNeary and Baskaran, 2003), varied from 0.0003 to 0.018 dpm cm^{-2} year^{-1} (mean: 0.0076 ± 0.0055, n = 13 for ^{210}Po; note: here and elsewhere the error is 1σ on data) and 0.018 to 0.68 dpm cm^{-2} year^{-1} (mean: 0.22 ± 0.05, n = 13 for ^{210}Pb; **Table 1**).

$$F_{Po\ or\ Pb}(\text{dpm cm}^{-2}\text{year}^{-1}) = C_{Po}(\text{or } C_{Pb}, \text{dpm cm}^{-3}\text{air}) \times V_d(\text{cm y}^{-1}) \quad (1)$$

The calculated depositional fluxes critically depend on the assumed V_d value of 1 cm s^{-1}. An independent validation for V_d in the Arctic can be obtained from the published F_{Pb} values. From the summarized sedimentary inventory of F_{Pb} in lakes, coastal regions and glaciers/ice cores, the calculated V_d ranged from 0.3 to 1.6 cm s^{-1} (mean: 0.9 ± 0.4 cm s^{-1} (n = 13)), indicating V_d for Arctic is similar to subarctic (Turekian et al., 1977; McNeary and Baskaran, 2003).

The residence time of aerosols (τ_{Po-Pb}) has been calculated from the measured ^{210}Po-^{210}Pb disequilibrium using the equation (Moore et al., 1973).

$$\tau_{Po-Pb} = [-b + (b^2 - 4ac)^{1/2}]/2a \quad (2)$$

where a = A_{Pb} – A_{Po}; b = -A_{Po} (τ_{Bi} + τ_{Po}) and c = -A_{Po} (τ_{Bi} τ_{Po}); A_{Pb} and A_{Po} are activities of ^{210}Po and ^{210}Pb respectively; τ_{Bi}: ^{210}Bi mean-life, 7.2 days; τ_{Po}: ^{210}Po mean-life, 199.7 days. The ^{210}Po/^{210}Pb AR in aerosols varied between 0.003 and 0.077 (mean: 0.039 ± 0.026, n = 13) corresponding to a mean residence time of 12 ± 7 days which is comparable to the mean residence time of water vapor as well as the residence times reported in regions where anthropogenic inputs of ^{210}Po and ^{210}Pb were reported to be negligible (Moore et al., 1973; Baskaran and Shaw, 2001; Baskaran, 2011). If there are additional contributions of ^{210}Po from sources such as volcanic eruption, transport from urban setting, and other anthropogenic sources, the estimated residence time will be an upper estimate (Kim et al., 2000, 2005; Su and Huh, 2002; summarized in Baskaran, 2011).

Age of Snow Using ^{210}Po/^{210}Pb AR

During the sampling expedition, in each ice station, a composite sample was collected and the snow depth was not measured.

TABLE 3 | Activity of particulate (p), dissolved (d) and total (T) ^{210}Po and ^{210}Pb (in dpm 100L^{-1}), ^{210}Po/^{210}Pb activity ratio, and age of snow.

Station & Event #	ST-31; 6206	ST-33; 6230	ST-39; 6263	ST42; 6291	ST-43; 6316	ST-46; 6338
Location	88.42°N;183.33°W	89.96°N; 3.529°E	87.78°N 149.61°W	85.74°N 150.54°W	85.16°N 150.00 W	82.49°N 149.93°W
$^{210}Po_p$	220 ± 7	15.2 ± 0.5	2.85 ± 0.13	8.89 ± 0.35	13.1 ± 0.5	2.42 ± 0.11
$^{210}Po_d$	103 ± 3	112 ± 3	3.31 ± 0.12	21.9 ± 0.8	23.4 ± 0.9	7.40 ± 0.35
$^{210}Po_T$	323 ± 7	127 ± 3	6.16 ± 0.17	30.8 ± 0.9	36.6 ± 1.0	9.82 ± 0.36
$^{210}Pb_p$	265 ± 9	78.4 ± 3.0	33.9 ± 1.3	38.6 ± 1.5	27.1 ± 1.0	5.64 ± 0.23
$^{210}Pb_d$	1394 ± 51	872 ± 32	158 ± 5	238 ± 8	553 ± 19	469 ± 18
$^{210}Pb_T$	1659 ± 52	951 ± 32	192 ± 5	276 ± 8	580 ± 19	475 ± 17
$(^{210}Po/^{210}Pb)_T$	0.20 ± 0.01	0.13 ± 0.01	0.032 ± 0.001	0.11 ± 0.01	0.063 ± 0.003	0.021 ± 0.001
$(^{210}Po/^{210}Pb)_p$	0.83 ± 0.04	0.19 ± 0.01	0.084 ± 0.005	0.23 ± 0.01	0.48 ± 0.03	0.43 ± 0.03
*Age (d)	34 ± 2	20 ± 1	4.0 ± 0.3	15 ± 1	4.9 ± 0.6	1.7 ± 0.2

Age was calculated using eq. (3) with $(^{210}Po/^{210}Pb)_i$ = 0.039 ± 0.026 (for ST-31, 33, 42, and 43) average of 13 aerosol samples (Table 1**) and for ST-39 and 46 where $(^{210}Po/^{210}Pb)$ is <0.039, the $(^{210}Po/^{210}Pb)_i$ value of 0.0122 ± 0.0005 (average of the lowest 5 values in **Table 1**) was used.*

However, the average snow depth has been reported to vary from 30-40 cm, with up to 150 cm after a snowstorm (Sturm et al., 2002). The total ^{210}Po ($^{210}Po_T$ = particulate, ≥0.4 μm, $^{210}Po_p$ + dissolved, <0.4 μm, $^{210}Po_d$) and $^{210}Pb_T$ activities varied from 6 to 323 (mean: 89 ± 123, n = 6) and 192 to 1659 (mean: 689 ± 545, n = 6) dpm 100L^{-1} water equivalent, respectively (**Table 3**), about 1-2 orders of magnitude higher than those in Arctic surface ocean waters (Moore and Smith, 1986; Smith et al., 2003; Chen et al., 2012; Roca-Marti et al., 2016; Bam et al., 2020; **Figures 2A,B**). The particulate ^{210}Po fraction, 12.0 to 68.1% (mean: 36 ± 19%), is significantly higher than that of $^{210}Pb_p$, 1.2 to 17.7% (mean: 10.3 ± 6.6%, **Table 3**). The observed higher fraction of $^{210}Po_p$ in snow (and melt pond and ice cores) is intriguing as it may be due to production of higher amounts of gelatinous exopolymeric substances (EPS) by microorganisms underneath the snow which serve as agents for increased primary productivity (Krembs et al., 2011). Laboratory experiments have shown that Po strongly adsorbed on to biogenic organic matter such as chitin compared to lithogenic elements such as Pb and, with fractionation factor (=K_d^{Po}/K_d^{Pb} ratio; K_d, partition coefficient = (particulate activity/dissolved activity)* (1/particulate concentration, μg/L)) of ∼4 compared to 0.2 to 1.0 for commonly occurring clay minerals (Fowler, 2011; Yang et al., 2013; Wang et al., 2019). Since no measurements of POC, macronutrients or pigments were made on collected snow or ice or melt pond samples, we cannot corroborate this hypothesis. Note that the higher fraction of $^{210}Po_p$ has no bearing on the age determination, as age calculation involves only total ^{210}Po ($^{210}Po_T$) and total ^{210}Pb ($^{210}Pb_T$) (see below). The $(^{210}Po/^{210}Pb)_p$ ARs varied from 0.08 to 0.83 (mean: 0.38 ± 0.27) which are significantly higher than that in the dissolved phase (range: 0.016 to 0.128, mean: 0.062 ± 0.044; calculated from data in **Figures 3A,B** and **Table 3**).

The age of snow (and ice core, melt pond or IRS) can be obtained from eq. (3). Age of snow refers to time elapsed between the snow fall to the ground and sample collection; age of ice core is the time elapsed between the formation of ice core and sample collection; age of melt pond is the time elapsed between the formation of melt pond and the sample collection; and age of ice-rafted sediment (IRS) is the time elapsed between the incorporation of excess ^{210}Pb in to the sediment and the time of collection IRS. The age can be obtained from eq. (3):

$$t = (-1/\lambda)[\ln(1-(^{210}Po/^{210}Pb)_T - (^{210}Po/^{210}Pb)_i)] \quad (3)$$

The $(^{210}Po/^{210}Pb)_i$ is initial AR at the time of deposition, taken to be 0.039 ± 0.026, average (^{210}Po/^{210}Pb) AR of aerosols (n = 13, **Table 1**); λ is ^{210}Po decay constant (λ = 5.01 × 10^{-3} day^{-1}). Instead of taking average of 13 samples, taking a subset (station 4, 6-10), the initial ratio becomes 0.031 ± 0.029 and it made very little difference on the age of snow. Since there is large spatial and temporal variability on the activities of ^{210}Po and ^{210}Pb in aerosols, we chose to use the average of all 13 samples.

The age of snow obtained from eq. (3) varied between 1.7 to 34 days (mean: 13 ± 11 days, **Figure 4** and **Tables 1**, **3**).

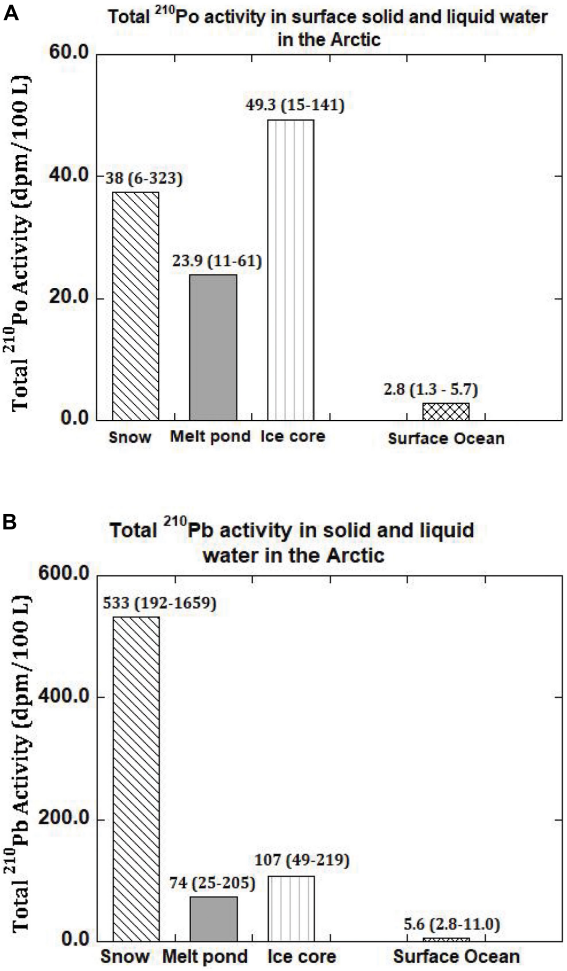

FIGURE 2 | (A) Activity of total (= particulate + dissolved) ^{210}Po and ^{210}Pb in snow, melt pond, ice core and surface ocean in the Arctic. The mean values are given and numbers in parenthesis denote the range (US GEOTRACES Arctic cruise, HLY 1502, R/V Icebreaker USCGC Healy). **(B)** Activity of total (= particulate + dissolved) ^{210}Pb and ^{210}Pb in snow, melt pond, ice core and surface ocean in the Arctic. The mean values are given and numbers in parenthesis denote the range (US GEOTRACES Arctic cruise, HLY 1502, R/V Icebreaker USCGC Healy).

If the analyzed snow is from multiple snow events at different times, then this is a composite age. The snowfall in the Arctic is highly patchy and no weather records are available for individual ice stations. The low-end age likely represents recent snow deposition. It is commonly assumed that once ^{210}Pb and ^{210}Po are delivered from the Arctic atmosphere to the air-sea interface through snowfall, they remain as a closed system and the changes in their activities are caused only by their radioactive decay as well as in-growth of ^{210}Po from the decay of ^{210}Pb until sample collection. This study shows generally that the age of snow is less than a month, and thus, snow deposited more than a month ago likely has undergone changes to become ice with associated exchange of heat energy with the surroundings. The implication of this study is that the changes in the ages

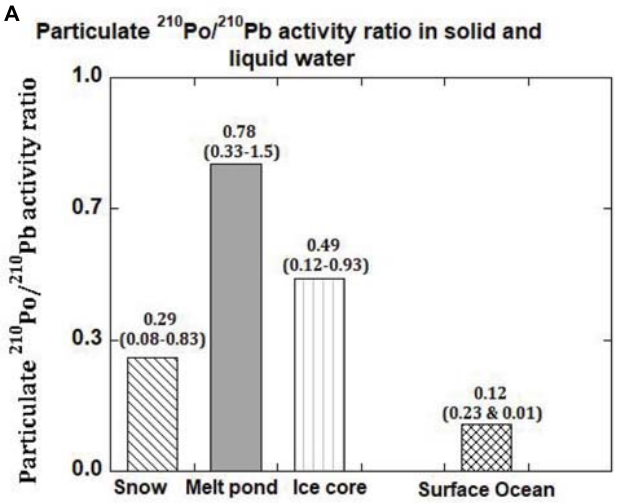

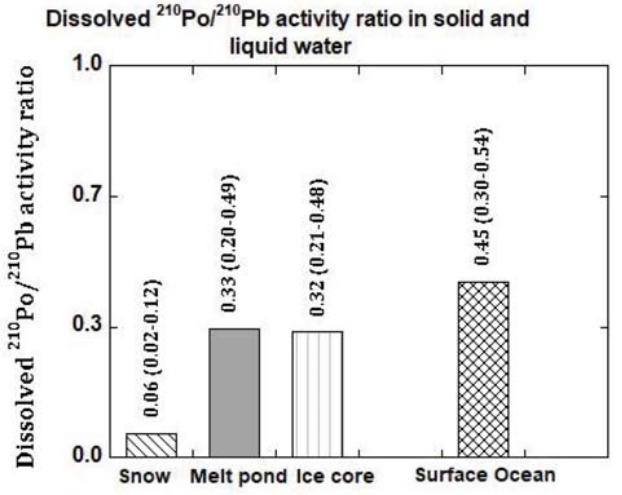

FIGURE 3 | (A) ^{210}Po/^{210}Pb activity ratio in the particulate matter in snow, melt pond, ice core and surface ocean in the Arctic. The mean values are given and numbers in parenthesis denote the range (US GEOTRACES Arctic cruise, HLY 1502, R/V Icebreaker USCGC Healy). **(B)** ^{210}Po/^{210}Pb activity ratio in the dissolved phase in snow, melt pond, ice core and surface ocean in the Arctic. The mean values are given and numbers in parenthesis denote the range (US GEOTRACES Arctic cruise, HLY 1502, R/V Icebreaker USCGC Healy).

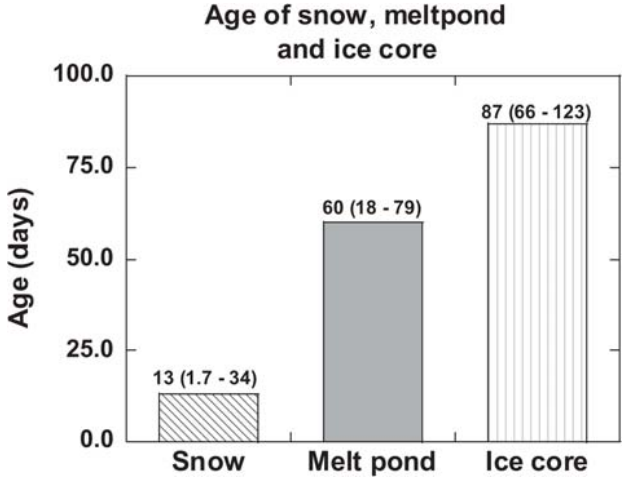

FIGURE 4 | ^{210}Po:^{210}Pb-disequilibrium-based age/residence time of snow, melt pond ice core and compared to the residence time of surface ocean water. The mean values are given and numbers in parenthesis denote the range (US GEOTRACES Arctic cruise, HLY 1502, R/V Icebreaker USCGC Healy).

of snow and ice due to global climate change (e.g., earlier melt and later freeze of ice) will affect the latent heat exchanged with the surroundings.

Age of Ice-Rafted Sediment Using $^{210}Po_{xs}/^{210}Pb_{xs}$ Activity Ratio

Sea ice in the Arctic plays an important role in the biogeochemical cycling of key trace metals, transport and subsequent dispersal of coastal sediments and nutrients to the deep Arctic as well as impacting radiation balance. Three proposed mechanisms for sediment entrainment into sea ice include: (i) incorporation of fine suspended sedimentary particles into frazil-ice crystals in shallow coastal areas; (ii) uplift of sediments by anchor ice; and (iii) discharge of river-borne ice-laden sediments into the sea (Reimnitz et al., 1987; Hebbeln and Weber, 1991; Nürnberg et al., 1994; Eicken et al., 1997). The concentration and composition of IRS, incorporated in coastal sea ice which are subsequently transported to the deep Arctic by the Beaufort Gyre and Transpolar Drift, has direct bearing on the albedo, long-range redistribution of contaminants, and particle flux to the deep sea (Hebbeln and Weber, 1991; Nürnberg et al., 1994; Pfirman et al., 1995; Eicken et al., 1997; Landa et al., 1997; Meese et al., 1997; Cooper et al., 1998; Charette et al., 2020).

The excess $^{210}Pb_{xs}$ activities ($^{210}Pb_{xs}$ = $^{210}Pb_{total}$ – ^{226}Ra; average measured ^{226}Ra: 0.95 ± 0.18) in IRS, range between 19 and 186 dpm g^{-1} (mean: 96 ± 76, **Table 4**), similar to earlier published data and is up to 2 orders of magnitude higher than the average total ^{210}Pb activity, 1.90 dpm g^{-1} (n = 134) of Russian Arctic surface sediments (Roberts et al., 1997; Baskaran, 2005). The $^{210}Po_{xs}$ ($^{210}Po_{xs}$ = $^{210}Po_{total}$ – ^{226}Ra) ranged from 5 to 76 dpm g^{-1} (mean: 40 ± 33, **Table 4**). This is the first ^{210}Po published data in IRS showing high ^{210}Po enrichment as well disequilibrium between ^{210}Po and ^{210}Pb. Note that enrichment of ^{210}Po onto particulate matter will not affect the total ^{210}Po/total ^{210}Pb activity ratio (total ^{210}Po = particulate ^{210}Po + dissolved ^{210}Po) of the ages calculated based on $^{210}Po/^{210}Pb$ activity ratio. The $^{210}Po_{xs}/^{210}Pb_{xs}$ AR varied from 0.27 to 0.50 (mean: 0.38 ± 0.09, n = 6) and the differences in the AR and enrichment of ^{210}Pb are attributed to the differences in their extent of initial interaction with seawater, and the time elapsed since the incorporation of ^{210}Pb into IRS.

Assuming the incorporation of atmospherically delivered ^{210}Pb into IRS is a one-time event (e.g., ^{210}Pb-laden sediment

TABLE 4 | Activities^{+} of excess ^{210}Po, ^{210}Pb, ^{210}Po/^{210}Pb AR and age of ice-rafted sediment.

Station	Location	^{210}Po (dpm/g)	^{210}Pb (dpm/g)	(^{210}Po/^{210}Pb) AR	"Age" (day)
E6195	87°45.1′ N	58.5 ± 1.9	118 ± 3	0.50 ± 0.02	122 ± 8
	179°43.4′W	76.4 ± 2.5	180 ± 6	0.42 ± 0.02	97 ± 7
		75.2 ± 2.8	186 ± 5	0.40 ± 0.02	88 ± 6
E6244	88°58.4′ N	10.5 ± 0.5	37.4 ± 1.8	0.28 ± 0.02	56 ± 4
	150°24.8′W	15.0 ± 0.7	35.6 ± 1.2	0.42 ± 0.03	96 ± 9
		5.18 ± 0.20	18.9 ± 0.7	0.27 ± 0.02	52 ± 5

$^{+}$^{226}Ra activity of 0.95 ± 0.18 dpm g^{-1} was subtracted from total ^{210}Po and ^{210}Pb activities. Errors associated with activity in all Tables are propagated error arising from counting statistics, error associated with the spike and reagent blank.

incorporation in to sea ice sediment taking place in one freeze over a short period of time), and the ^{210}Po and ^{210}Pb in IRS remains a closed system, the calculated age ranged from 52 to 122 days (mean = 85 ± 27 days, n = 6, **Table 4**). Although there is no direct observation from the Arctic for this assumed one-time incorporation of radionuclides, a serendipitous observation from collection and analysis of sediment-laden ice from Lake St. Clair in southeast Michigan showed that the sediment extracted from ice during a snow storm during March 14-15, 2015 had an average ^{210}Pb$_{xs}$ activity of 555 ± 138 (n = 3) dpm g^{-1} (Krupp, 2017). This is ∼6 times higher than that in the Arctic and about 100 times that of surficial sediments in Lake St. Clair (Robbins et al., 1990; Jweda and Baskaran, 2011). Note that the average atmospheric depositional flux of ^{210}Pb in 60-80°N belt of 0.18 dpm cm^{-2} year^{-1} is only 13% as that of Detroit, MI (1.41 dpm cm^{-2} year^{-1}), a mid-latitude site, and such larges differences are due to low emanation rate of ^{222}Rn as well as low annual amount of precipitation in the Arctic (McNeary and Baskaran, 2003; Baskaran, 2011). The corresponding transport velocities (transport velocity = shortest distance between sampling site and the nearest coastal site, taking in to consideration the currents in the sampling area and back tracked the trajectory of the ice since its formation/age) varied between 0.12 ± 0.01 and 0.27 ± 0.02 m s^{-1} (mean: 0.18 ± 0.06 m^{-1}, **Table 4**). These velocities can be compared to 0.082-0.086 m s^{-1} obtained using buoys in Laptev Sea and 0.09 ± 0.04 m s^{-1} (range: 0.04-0.18 m s^{-1}, n = 23, monthly, April 1996 – February 1998) over Eastern Beaufort Sea using Acoustic Doppler Current Profiler (Melling and Riedel, 2003). Note that the calculated velocities are based on ^{210}Po/^{210}Pb initial AR value of 0.039 (**Table 1**) and if AR is higher due to significant contribution of ^{210}Po from resuspension of superfine sedimentary material with initial AR > 0.039, then, the age will be lower and the transport velocities will be higher.

Dating of Melt Pond Using ^{210}Po/^{210}Pb AR

During late spring and early summer, melt from snow (meteoric water) and surface ice (ice core salinity range: 0-5.2 ppt, surface to 169 cm, **Supplementary Figure 1**) mixing with a fraction of surface seawater result in the formation of melt ponds. The melt ponds are generally darker compared to ice leading to more absorption of incident radiation (lower albedo) compared to snow and ice. Furthermore, the vertical and horizontal fluxes of melt water from snow and ice play a key role in the evolution of albedo, heat transfer, and mass balance of the Arctic ice pack (Eicken, 1994; Eicken et al., 2002; Perovich et al., 2003). Surface area and depth of the melt ponds were not recorded during the field expedition; however, an average surface area of 30 m^2 and depth of 0.2 m have been reported (Eicken et al., 2002). The fractions of these three contributing sources to these melt ponds were estimated using a three end-member mixing model using salinity, δ^{18}O and ^{7}Be data (Marsay et al., 2018; **Table 5**).

The activities of ^{210}Po$_p$ range from 0.4 to 4.0 (mean: 1.7 ± 0.2 dpm 100L^{-1}, n = 5) while the corresponding ^{210}Pb$_p$ range from 0.3 to 5.6 (mean: 2.6 ± 0.4 dpm 100L^{-1}, n = 5) which are comparable to values in Arctic surface waters (Moore and Smith, 1986; Smith et al., 2003; Roca-Marti et al., 2016; Bam et al., 2020). However, the ^{210}Po$_T$ range from 11 to 61 (mean: 28 ± 3, n = 5) dpm 100L^{-1} and ^{210}Pb$_T$ range from 25 to 205 (mean: 94 ± 8, n = 5) dpm 100L^{-1}, which are about 5 to 10 times higher than those found in surface seawater from the same or nearby stations (**Figures 2A,B** and **Table 5**). Such differences between particulate and total activities are attributed to differences in the sources of water to the melt ponds, with differences in the activities between the three source waters (**Figures 2A,B** and **Table 5**). The activities of ^{210}Po$_T$ and ^{210}Pb$_T$ at the time of melt pond formation were calculated using three end-member (snow, ice, and surface seawater) mixing model, as given in (eq. 4). The initial (^{210}Po$_T$/^{210}Pb$_T$) AR varied between 0.071 and 0.143 (n = 4); however, in ST-39, the ratio is >1.0.

$$\text{Activity of } {}^{210}\text{Po}_\text{T} (\text{or } {}^{210}\text{Pb}_\text{T}) \text{ at the beginning of melt pond formation} = (F^{*}_{\text{snow}}\,{}^{210}\text{Po}_{\text{T-snow}}) + (F^{*}_{\text{sw}}\,{}^{210}\text{Po}_{\text{T-sw}}) + (F^{*}_{\text{ice}}\,{}^{210}Po_{T-\text{ice}}) \quad (4)$$

and likely the assumptions are not well constrained; taking the initial AR to be the same as that of the aerosols (**Table 1**), we get an age of 75 ± 9 days, although no other rationale can be given for using this ratio. Assuming the melt pond was formed in a relatively short timescale compared to the age of the pond, its age calculated using eq. (3) varied between 18 ± 3 and 79 ± 6 days (mean: 60 ± 14 days, n = 4, **Table 5**). If this assumption is not strictly valid, then, the calculated age reported in **Table 5** is an overestimate. The ages (**Figure 4** and **Table 5**) indicate that ST-33 pond formed in late spring while ST-42, 43 in early summer and ST-46 in mid-summer.

If the particulate matter present in some of the melt ponds had undergone multiple melt-freeze cycles spanning over more than a year, then, we expect secular equilibrium between ^{210}Po$_p$ and ^{210}Pb$_p$ with ^{210}Po$_p$/^{210}Pb$_p$ AR ∼ 1.0, under a closed system for ^{210}Po and ^{210}Pb. In two samples where (^{210}Po/^{210}Pb)$_p$ AR is >1.0, the particulate matter could have undergone multiple melt-freeze cycles although we have no

TABLE 5 | *Activities of ^{210}Po and ^{210}Pb (dpm/100 L), fractional amounts snow (F_{snow}), ice (F_{ice}), and seawater (F_{sw}), and age** of melt ponds.

Station	33	39	42	43	46
$^{210}Po_p$	1.88 ± 0.09	0.90 ± 0.06	1.46 ± 0.09	0.40 ± 0.03	4.02 ± 0.16
$^{210}Po_d$	9.35 ± 0.41	20.3 ± 0.8	18.5 ± 0.8	61.0 ± 3.1	22.6 ± 1.0
$^{210}Po_T$	11.2 ± 0.4	21.2 ± 0.8	20.0 ± 0.9	61.4 ± 3.1	26.6 ± 1.0
$^{210}Pb_p$	5.62 ± 0.24	0.92 ± 0.06	3.46 ± 0.18	0.28 ± 0.03	2.70 ± 0.11
$^{210}Pb_d$	18.9 ± 0.7	60.1 ± 2.5	59.7 ± 2.1	204 ± 7	112 ± 5
$^{210}Pb_T$	24.6 ± 0.8	61.0 ± 2.5	63.2 ± 2.1	205 ± 7	115 ± 5
$(^{210}Po/^{210}Pb)_p$ AR	0.33 ± 0.02	0.98 ± 0.09	0.43 ± 0.03	1.40 ± 0.02	1.50 ± 0.10
Salinity	1.4	10.6	5.92	25.76	4.49
F_{snow}	0.94	0.21	0.24	0.21	0.2
F_{sw}	0.04	0.25	0.09	0.79	0.03
F_{ice}	0.02	0.54	0.67	0	0.77
$^{210}Po_{T-snow}$	127 ± 3	61.6 ± 0.2	30.8 ± 0.9	36.6 ± 1.0	9.82 ± 0.36
$^{210}Po_{T-sw}$	0.99 ± 0.08	0.99 ± 0.08	1.34 ± 0.12	1.34 ± 0.12	1.34 ± 0.12
$^{210}Po_{T-ice}$	31.1 ± 1.0	141 ± 4	15.1 ± 0.7	112 ± 4	23.8 ± 0.9
$^{210}Pb_{T-snow}$	951 ± 32	192 ± 5	276 ± 8	580 ± 19	475 ± 17
$^{210}Pb_{T-sw}$ (dpm/100 L)	3.28 ± 0.28	3.28 ± 0.28	2.82 ± 0.12	2.82 ± 0.12	2.82 ± 0.12
$^{210}Pb_{T-ice}$ (dpm/100 L)	86.9 ± 2.4	49 ± 1.7	131 ± 5	219 ± 6	61.5 ± 2.1
Calculated $^{210}Po_T$	120 ± 3	78 ± 2	17.6 ± 0.5	8.7 ± 0.2	20.3 ± 0.7
Calculated $^{210}Pb_T$	896 ± 30	68 ± 1	154 ± 4	124 ± 4	142 ± 3.8
$(^{210}Po/^{210}Pb)_i$ AR (calculated)+	0.134 ± 0.005	1.15 ± 0.04	0.114 ± 0.004	0.071 ± 0.003	0.143 ± 0.006
$(^{210}Po/^{210}Pb)_T$ AR (measured)	0.46 ± 0.02	0.35 ± 0.02	0.32 ± 0.02	0.30 ± 0.02	0.23 ± 0.01
AR-measured-initial	0.326 ± 0.020	0.311 ± 0.033	0.206 ± 0.020	0.229 ± 0.020	0.087 ± 0.012
Age** (days)	79 ± 6	75 ± 9	46 ± 5	52 ± 5	18 ± 3

** p, particulate; d, dissolved; T, total (=particulate + dissolved), sw: seawater; for sw $^{210}Po_T$ and $^{210}Pb_T$, ST-33 surface water values were used for ST-39; for ice stations 42 and 46, ST-43 surface seawater values were used; data from Krupp (2017).*

***Ages for ST-33, 42, 43 and 46 were calculated from calculated initial and measured. $(^{210}Po/^{210}Pb)_T$ AR. In the calculation for ST-39, $(^{210}Po/^{210}Pb)$ AR was assumed to the same as in aerosols (0.039 ± 0.026) and yields an age of 75 ± 9 days, which is a lower estimate (see in the text). Fractional values of F_{snow}, F_{sw} and F_{ice} are taken from Marsay et al. (2018). Calculated ^{210}Po (or ^{210}Pb) is the activity at the time of formation of melt pond = $(F_{snow}{}^{*210}Po_{T-snow}) + (F_{sw}{}^{210}Po_{T-sw}) + (F_{ice}{}^{*210}Po_{T-ice})$. + calculated AR value for ST 33, 42, 43 and 46 is assumed to be the initial AR at the time of formation of melt pond using eq. (4). For ST-39, $^{210}Po/^{210}Pb$ AR is 1.15 ± 0.04 and is not well constrained by the 3-end-member mixing model.*

other supporting evidence (**Figure 3A** and **Table 5**). Note that average particulate fraction of ^{210}Po is only 8.8% (range: 0.7-16.7%), and even if some of the particulate matter is derived from multiple melt-freeze cycles that will not affect the $(^{210}Po/^{210}Pb)_T$ AR-based-ages. However, in 3 samples $(^{210}Po/^{210}Pb)_p$ AR is < 1.0 and $(^{210}Po/^{210}Pb)_T$ AR is <1.0 in all 5 samples (**Table 5**).

Activity of ^{210}Po and ^{210}Pb, Their AR and Dating of Ice Core

The $^{210}Po_{p,d}$ and $^{210}Pb_{p,d}$ activities in the upper segment of 6 ice cores varied by more than an order of magnitude, from 4.4 to 75 dpm $100L^{-1}$ for $^{210}Po_p$ and 11 to 120 dpm 100 L^{-1} for $^{210}Pb_p$ and 11 to 96 dpm $100L^{-1}$ for $^{210}Po_d$ and 0.8 to 174 dpm 100 L^{-1} for $^{210}Pb_d$. The activities of particulate, dissolved and total phases varied over two orders of magnitude in all 31 split samples (**Table 6**), similar to an earlier study (Masqué et al., 2007). Although there is no excess ^{210}Po (i.e., $^{210}Po/^{210}Pb$ AR < 1.0) in the inventory-based particulate or dissolved phases (**Table 7**), excess $^{210}Po_d$ (and $^{210}Po_T$) were observed in three discrete layers: ST-31 (100-130 cm), ST-33 (84-112 cm), and ST-39 (0-38 cm); the $(^{210}Po/^{210}Pb)_T$ AR in those layers ranged between 2.88 and 4.58 (**Table 6**), indicating preferential sorption of ^{210}Po and/or preferential loss of ^{210}Pb. This contrasts with observed ^{210}Po-^{210}Pb equilibrium in 87%, (within ± 1σ) of the 38 segments from two ice cores from Fram Strait, although reported associated errors in majority of the samples were high in Masqué et al. (2007).

If the accumulation and ablation of ice takes place uniformly, with accretion from the top and ablation from the bottom, the $(^{210}Po/^{210}Pb)_T$ AR profile is expected to increase with increasing depth; however, when multiple processes such as meltwater deformation, seawater congelation, and false bottom formation takes place, the measured $(^{210}Po/^{210}Pb)_T$ AR will result in a more complicated profile. If a multi-year (≥2 year) ice is present, the $(^{210}Po/^{210}Pb)_T$ AR is expected to be ∼1.0 under the assumption that the ^{210}Po-^{210}Pb has remained a closed system. We contend that ice that are >2 year old should have an $^{210}Po_p/^{210}Pb_p$ AR of ∼1.0, because any disequilibrium broken earlier in the decay chain will adjust to radioactive secular equilibrium in about two years, and thus paving the way to delineate >1 year old ice from more recent ones. The $^{210}Po/^{210}Pb$ AR of 0.95 ± 0.07 in only one sample (ST-30, 60-80 cm, **Table 6**) could be a part of multi-year ice segment; thus, we report the ice samples we collected are mostly first-year ice, with $^{210}Po/^{210}Pb$

TABLE 6 | Dissolved, particulate, total activities and activity ratios for ice station samples.

ST & Event	Ice Core Depth (cm)	$^{210}Po_p$ dpm 100L^{-1}	$^{210}Po_d$ dpm 100L^{-1}	$^{210}Po_T$ dpm 100L^{-1}	$^{210}Pb_p$ dpm 100L^{-1}	$^{210}Pb_d$ dpm 100L^{-1}	$^{210}Pb_T$ dpm 100L^{-1}	$^{210}Po_T/^{210}Pb_T$ AR
ST-31 6205								
	0-20	20.9 ± 1.0	60.0 ± 2.2	80.9 ± 2.4	28.0 ± 1.1	174 ± 6	202 ± 6	0.40 ± 0.02
	20-40	5.59 ± 0.39	10.9 ± 0.6	16.4 ± 0.7	13.7 ± 0.6	72.1 ± 2.9	85.8 ± 3.0	0.19 ± 0.01
	40-60	1.36 ± 0.11	2.55 ± 0.19	3.91 ± 0.22	3.23 ± 0.20	11.9 ± 0.6	15.2 ± 0.6	0.26 ± 0.02
	60-80	1.89 ± 0.16	5.21 ± 0.34	7.10 ± 0.37	1.24 ± 0.08	6.23 ± 0.41	7.47 ± 0.41	0.95 ± 0.07
	80-100	1.04 ± 0.10	1.72 ± 0.13	2.75 ± 0.16	BDL	3.52 ± 0.25	3.52 ± 0.25	0.78 ± 0.07
	100-130	0.94 ± 0.09	2.70 ± 0.20	3.63 ± 0.22	0.031 ± 0.002	1.09 ± 0.09	1.12 ± 0.09	3.25 ± 0.32
ST-33; Event #: 6238								
	0-28	17.4 ± 0.8	13.7 ± 0.6	31.1 ± 1.0	37.1 ± 1.4	49.8 ± 1.9	86.9 ± 2.4	0.36 ± 0.01
	28-56	3.23 ± 0.22	40.2 ± 1.8	43.5 ± 1.8	2.09 ± 0.14	45.3 ± 1.8	47.4 ± 1.8	0.92 ± 0.05
	56-84	2.33 ± 0.15	1.52 ± 0.11	3.85 ± 0. 0.19	2.15 ± 0.14	6.09 ± 0.38	8.24 ± 0.41	0.47 ± 0.03
	84-112	0.25 ± 0.02	1.23 ± 0.10	1.48 ± 0.10	BDL	0.32 ± 0.03	0.32 ± 0.03	4.58 ± 0.51
	112-140	0.84 ± 0.07	3.60 ± 0.21	4.44 ± 0.23	1.11 ± 0.08	16.7 ± 0.8	17.8 ± 0.8	0.25 ± 0.02
ST-39; Event #: 6271								
	0-38	44.8 ± 3.7	96.3 ± 3.3	141 ± 4	48.2 ± 1.7	0.78 ± 0.13	49.0 ± 1.7	2.88 ± 0.12
	38-76	3.67 ± 0.22	20.5 ± 0.9	24.2 ± 0.9	15.7 ± 0.7	59.7 ± 2.5	75.4 ± 2.6	0.32 ± 0.02
	76-114	2.67 ± 0.17	9.97 ± 0.47	12.6 ± 0.5	4.26 ± 0.21	72.7 ± 2.8	77.0 ± 2.8	0.16 ± 0.01
	114-152	2.70 ± 0.23	5.10 ± 0.33	7.81 ± 0.41	7.03 ± 0.43	25.1 ± 1.5	32.1 ± 1.5	0.24 ± 0.02
	152-190	3.99 ± 0.25	7.64 ± 0.47	11.6 ± 0.5	10.7 ± 0.75	20.2 ± 0.9	31.0 ± 1.2	0.38 ± 0.02
ST-42; Event #: 6292								
	0-20	4.46 ± 0.29	10.7 ± 0.6	15.1 ± 0.7	36.6 ± 1.9	94.2 ± 4.1	131 ± 5	0.12 ± 0.01
	20-40	7.37 ± 0.49	6.63 ± 0.44	14.0 ± 0.7	20.0 ± 1.0	30.9 ± 1.5	50.9 ± 1.8	0.28 ± 0.02
	40—60	14.1 ± 0.8	10.8 ± 0.6	24.9 ± 0.9	24.4 ± 1.1	34.7 ± 1.7	59.2 ± 2.0	0.42 ± 0.02
	60-80	4.51 ± 0.37	3.37 ± 0.27	7.88 ± 0.46	5.28 ± 0.35	16.8 ± 1.0	22.0 ± 1.1	0.36 ± 0.03
	80-100	2.64 ± 0.23	4.74 ± 0.33	7.38 ± 0.41	6.22 ± 0.44	28.1 ± 1.8	34.3 ± 1.8	0.21 ± 0.02
ST-43; Event #: 6323								
	0-33	74.7 ± 3.2	37.2 ± 1.8	112 ± 4	120 ± 5	99.3 ± 3.5	219 ± 6	0.51 ± 0.02
	33-66	7.43 ± 0.39	12.2 ± 0.7	19.6 ± 0.8	14.3 ± 0.7	26.7 ± 1.4	41.0 ± 1.5	0.48 ± 0.03
	66-99	2.10 ± 0.16	8.15 ± 0.41	10.2 ± 0.4	6.50 ± 0.39	46.3 ± 1.7	52.8 ± 1.7	0.19 ± 0.01
	99-132	0.97 ± 0.08	1.37 ± 0.12	2.34 ± 0.14	0.13 ± 0.01	3.52 ± 0.24	3.65 ± 0.24	0.64 ± 0.06
	132-165	1.58 ± 0.12	4.48 ± 0.28	6.06 ± 0.30	1.64 ± 0.12	16.8 ± 1.9	18.4 ± 1.9	0.33 ± 0.04
ST-46; GT # 11717								
	0-34	5.71 ± 0.34	18.1 ± 0.8	23.8 ± 0.9	10.7 ± 0.6	50.9 ± 2.0	61.5 ± 2.1	0.39 ± 0.02
	34-68	2.36 ± 0.18	5.53 ± 0.37	7.89 ± 0.41	5.78 ± 0.36	15.9 ± 1.7	21.6 ± 1.8	0.36 ± 0.04
	68-102	0.37 ± 0.03	3.21 ± 0.24	3.57 ± 0.24	1.96 ± 0.15	11.9 ± 0.8	13.8 ± 0.8	0.26 ± 0.02
	102-136	0.26 ± 0.03	1.73 ± 0.16	1.99 ± 0.16	0.011 ± 0.001	7.80 ± 0.66	7.81 ± 0.66	0.25 ± 0.03
	136-170	0.53 ± 0.04	2.35 ± 0.18	2.88 ± 0.19	0.87 ± 0.07	7.26 ± 0.45	8.13 ± 0.45	0.35 ± 0.03

BDL = below detection level; activity of sample was lower than the average blank level.

ARs ranging between 0.12 ± 0.01 and 0.78 ± 0.07 (n = 25, **Table 6**).

The inventory-based (=Σ activities in each segment of the ice core, dpm/Σ volume of melt water, L) activities of $^{210}Po_p$, $^{210}Pb_p$, $^{210}Po_d$ and $^{210}Pb_d$ varied widely: $^{210}Po_p$, varied about an order of magnitude, from 1.8 to 17.4 (mean: 8.1 ± 5.8, n = 6) dpm 100L^{-1}; $^{210}Po_T$ varied within a factor of ∼3, from 7.9 to 26.2 (mean: 18.8 ± 6.4, n = 6, calculated from **Table 7**) dpm 100L^{-1}. The range of $^{210}Pb_p$ activities is similar to $^{210}Po_p$, from 3.8 to 28.5 (mean: 14.3 ± 9.2, n = 6) dpm 100L^{-1}, while the corresponding values for $^{210}Pb_T$ varied within a factor of ∼3, from 22 to 69 (mean: 49 ± 18, n = 6, dpm 100L^{-1}). These values are almost an order of magnitude higher than those for the Arctic surface waters (**Figures 2A,B** and **Tables 6**, **7**), suggesting a significant fraction of the source of water is from snow melt and possibly some recycled component of melt ponds. During spring and summer, melt pond water can percolate through the depth of the ice floe forming a lens of super-cooled freshwater at the interface between the ice floe and surface seawater, which ultimately grows into a horizontal ice sheet known as false-bottom ice (Eicken, 1994; Eicken et al., 1997; Polashenski et al., 2012) and thus the signature of the melt pond could have been be imprinted on bottom ice. It seems this is a novel observation presenting a radioisotope-based evidence that the ice core derived some component of water from snow.

TABLE 7 | Calculated inventory-based particulate (p) and total (T = p + d) activity of ^{210}Po and ^{210}Pb and their activity ratio in whole ice core collected during US GEOTRACES Arctic cruise (HLY 1502).

Parameter	ST-31	ST-33	ST-39	ST42	ST-43	ST-46
Core length (cm)	115	126	171	90	149	153
Melt volume (L)	11.6	14.5	17.5	9.8	17.5	18.25
$^{210}Po_p$ (dpm/100 L)*	5.44 ± 0.19	4.86 ± 0.17	12.7 ± 0.8	6.66 ± 0.22	17.4 ± 0.6	1.82 ± 0.08
$^{210}Po_T$ (dpm/100 L)*	19.7 ± 0.4	15.9 ± 0.4	23.6 ± 0.9	19.4 ± 0.5	26.2 ± 0.7	7.89 ± 0.20
$^{210}Pb_p$ (dpm/100 L)*	7.96 ± 0.22	8.71 ± 0.29	18.2 ± 0.4	18.8 ± 0.5	28.5 ± 1.0	3.81 ± 0.14
$^{210}Pb_T$ (dpm/100 L)*	54.3 ± 2.2	31.6 ± 1.9	69.0 ± 1.7	61.0 ± 1.7	57.4 ± 2.2	22.2 ± 0.3
$(^{210}Po/^{210}Pb)_p$	0.68 ± 0.02	0.56 ± 0.02	0.70 ± 0.05	0.36 ± 0.01	0.61 ± 0.02	0.48 ± 0.02
$(^{210}Po/^{210}Pb)_T$	0.36 ± 0.01	0.50 ± 0.02	0.34 ± 0.01	0.32 ± 0.01	0.46 ± 0.02	0.36 ± 0.01
**Age (days)	77 ± 3	123 ± 8	72 ± 3	66 ± 3	109 ± 7	77 ± 3

*Activities of individual layers are given in **Table 6**. The particulate and total activities were calculated from the summation of the corresponding activity in each layer and divided by total melt volume of water for each core.*

***In the calculation of the age, the average of 13 aerosol initial $(^{210}Po/^{210}Pb)_i$ value of 0.039 ± 0.026 was used.*

The $(^{210}Po/^{210}Pb)_p$ AR for the whole ice core varied between 0.36 and 0.70 (mean: 0.56 ± 0.13, n = 6) which is significantly higher than the range of values and mean for $(^{210}Po/^{210}Pb)_T$ AR, 0.32 to 0.50 (mean: 0.39 ± 0.07, n = 6, **Table 7**). The higher $(^{210}Po/^{210}Pb)_p$ AR compared to $(^{210}Po/^{210}Pb)_d$ and $(^{210}Po/^{210}Pb)_T$ are similar to snow and melt pond, confirming enrichment of ^{210}Po in particulate matter. The calculated composite ages of the ice core, based on the inventory of $^{210}Po_T$ and $^{210}Pb_T$ and assuming initial $(^{210}Po/^{210}Pb)$ AR = 0.039, ranged between 66 and 123 days (mean: 87 ± 23 days; **Figure 4** and **Table 7**). If the initial ARs are higher, the calculated ages are upper limits.

CONCLUSION AND FUTURE OUTLOOK

We measured the disequilibrium between ^{210}Po and ^{210}Pb in a suite of aerosols and ice-rafted sediment as well in particulate and dissolved phases of snow, water from melt pond and surface seawater. We report, for the first time, highly elevated levels of ^{210}Po in biogenic particulate matter in snow and melt pond compared to ^{210}Pb indicating biogeochemical cycling of biogenic elements such as polonium is different in the Arctic. We also report one to two orders of magnitude higher ^{210}Pb and ^{210}Po activities in ice-rafted sediments (IRS) compared to benthic source sediments which indicate that the sea ice-sediment (i.e., IRS) is a powerful vector in the transport of land- and atmospherically delivered particle-reactive contaminants from the coastal area to the deep Arctic. Furthermore, transport of ice-rafted sediments through sea ice is one of the major mechanisms by which coastal sediments are transported and dispersed in the deep Arctic (during melt season) and nutrients associated with coastal sediments serve as food resource for deep benthic organisms in the open Artic, thus indicating coupling between coastal and deep arctic benthic ecosystems. The key findings are given below:

(i) From the measured ^{210}Po/^{210}Pb AR in snow and using the mean AR in aerosol as the initial AR in snow, the calculated age of snow collected from 6 different ice stations varied between 1.7 and 34 days (mean: 13 days);
(ii) The ages of 5 different melt ponds, based on the measured ^{210}Po/^{210}Pb AR and three end-member mixing modeling, ranged between 18 and 79 days (mean: 60 days). The activities of ^{210}Po and ^{210}Pb in melt-ponds is about 10 times higher compared to the surface seawater in the Arctic Ocean;
(iii) From the measured ^{210}Po-^{210}Pb activities in aerosols, collected from 13 different stations covering the entire 10 weeks of Western Arctic GEOTRACES cruise track from Dutch Harbor, AK to the North Pole, we show that the mean ^{210}Po/^{210}Pb activity ratio (AR) of 0.039 ± 0.026 (n = 13) corresponds to a residence time of 12 ± 7 days;
(iv) The transport velocity of the ice-rafted sediment in the shelf and interior Arctic Ocean, estimated based on the age obtained using ^{210}Po/^{210}Pb AR, 0.12 and 0.27 m/s, (mean: 0.18 ± 0.06 m/s) agree with the data obtained using buoys and Acoustic Doppler current profiler; and
(v) The ^{210}Po/^{210}Pb AR serves as a quantitative tool in delineating multiple-year ice from seasonal ice.

The residence time of snow and melt pond has direct bearing on the energy exchange between surface ocean and atmosphere as well as the heat exchange between Arctic and sub-arctic global oceans. The disequilibrium between ^{210}Po and ^{210}Pb provide not only a powerful tool in establishing chronology but also insight on the mechanism(s) of Po enrichment onto biogenic particulate matter. Routine identification of multi-year (those that survived more than one melt cycle) ice is now possible using ^{210}Po/^{210}Pb AR as a metric. Furthermore, long-term longitudinal study on the annual variations in the age of snow and melt pond in a particular region caused by climate change in the Arctic may enable us to quantify the radiation balance changes caused by faster melting of snow and later freeze. Highly enriched ^{210}Po in particulate matter in snow, ice and melt ponds suggest that the biological organisms play a key role in the enrichment of biogenic elements. The factors and processes that cause high enrichment of polonium in the particulate matter obtained from snow, ice and melt pond remains

unknown. A systematic study on the distribution of ^{210}Po and ^{210}Pb in particulate and dissolved phases along with characterization of particulate matter including quantification of acid polysaccharides and other biogenic molecular compounds will yield valuable information to understand the mechanisms of Po enrichment onto particulate matter in the Arctic.

DATA AVAILABILITY STATEMENT

The original data for this study are presented in the article/**Supplementary Material**. The data also can be obtained from https://www.bco-dmo.org/dataset/794064; and further inquiries can be directed to the corresponding author.

AUTHOR CONTRIBUTIONS

MB developed the idea, secured the funding, oversaw the project from conception to the end, and wrote most of the manuscript. KK participated in the cruise, collected and analyzed the samples, and interpreted the data. Both authors contributed to the article and approved the submitted version.

FUNDING

The work presented was a part of a master's thesis of KK. This work was supported by the National Science Foundation grant (NSF-PLR-1434578).

ACKNOWLEDGMENTS

We thank Captain, crew, and US GEOTRACES Western Arctic Management team for collection of water, snow, ice, and aerosol samples.

SUPPLEMENTARY MATERIAL

The Supplementary Material for this article can be found online at: https://www.frontiersin.org/articles/10.3389/fmars.2021.692631/full#supplementary-material

Supplementary Figure 1 | Vertical profiles of salinity in 5 ice cores.

REFERENCES

Bacon, M. P., Spencer, D. W., and Brewer, P. G. (1976). ^{210}Pb/^{226}Ra and ^{210}Po/^{210}Pb disequilibria in seawater and suspended particulate matter. *Earth Planet. Sci. Lett.* 32, 277–296.

Bam, W., Maiti, K., Baskaran, M., Krupp, K., Lam, P. J., and Xiang, Y. (2020). Variability of ^{210}Pb and ^{210}Po partition coefficients (K_d) along the US GEOTRACES Arctic Transect. *Mar. Chem.* 219:103749. doi: 10.1016/j.marchem.2020.103749

Baskaran, M. (2005). Interaction of sea ice sediments and surface sea water in the Arctic Ocean: Evidence from excess 210Pb. *Geophys. Res. Lett.* 32:L12601.

Baskaran, M. (2011). Po-210 and Pb-210 as atmospheric tracers and global atmospheric Pb-210 fallout: a Review. *J. Environ. Radioact.* 102, 500–513. doi: 10.1016/j.jenvrad.2010.10.007

Baskaran, M. (2016). *Applications of Radon progeny in atmospheric studies. In: Radon: A Tracer for Geological, Geophysical and Geochemical Studies*. Berlin: Springer.

Baskaran, M., Church, T. M., Hong, G.-H., Kumar, A., Qiang, M., Choi, H., et al. (2013). Effects of flow rates and composition of the filter, and decay-in-growth correction factors involved with the determination of in-situ particulate ^{210}Po and ^{210}Pb in seawater. *Limnol. Oceanogr. Methods* 11, 126–138. doi: 10.4319/lom.2013.11.126

Baskaran, M., and Shaw, G. E. (2001). Residence time of arctic haze aerosols using the concentrations and activity ratios of ^{210}Po, ^{210}Pb, and ^{7}Be. *J. Aerosol Sci.* 32, 17–26.

Carmack, E., and Chapman, D. C. (2003). Wind-driven shelf/basin exchange on the Arctic shelf: the joint roles of ice cover extent and shelf-break bathymetry. *Geophys. Res. Lett.* 30:1778.

Charette, M. A., Kipp, L. E., Jensen, L. T., Dabrowski, J. S., Whitmore, L. M., Fitzsimmons, J. N., et al. (2020). The transpolar drift as a source of riverine and shelf-derived trace elements to the Central Arctic Ocean. *J. Geophys. Res.* 125:e2019JC01520.

Chen, M., Ma, Q., Guo, L. D., Qiu, Y., Li, Y., and Yang, W. (2012). Importance of lateral transport processes to ^{210}Pb budget in the eastern Chukchi Sea during summer 2003. *Deep-Sea Res. II* 81-84, 53–62. doi: 10.1016/j.dsr2.2012.03.011

Cochran, J. K., and Masque, P. (2003). Short-lived U/Th-series radionuclides in the ocean: tracers for scavenging rates, export fluxes and particle dynamics. *Rev. Mineral. Geochem.* 52, 461–492. doi: 10.2113/0520461

Conan, F., and Robertson, L. B. (2002). Latitudinal distribution of radon-222 flux from continents. *Tellus* 54B, 127–133. doi: 10.1034/j.1600-0889.2002.00365.x

Cookbook (2014). *Sampling and Sample-handling Protocols for GEOTRACES Cruises*. Available Online at: http://www.geotraces.org/images/stories/documents/intercalibration/Cookbook_v2.pdf

Cooper, L. W., Larsen, I. L., Beasley, T. M., Dolvin, S. S., Grebmeier, J. M., Kelley, J. M., et al. (1998). The distribution of radiocesium and plutonium in sea ice-entrained Arctic sediments in relation to potential sources and sinks. *J. Environ. Radioact.* 39, 279–303. doi: 10.1016/s0265-931x(97)00058-1

Eicken, H. (1994). Structure of under-ice melt ponds in the Central Arctic and their effect on sea-ice cover. *Limnol. Oceanogr.* 39, 682–694. doi: 10.4319/lo.1994.39.3.0682

Eicken, H., Krouse, H. R., Kadko, D., and Perovich, D. K. (2002). Tracer studies of pathways and rates of meltwater transport through Arctic summer sea ice. *J. Geophys. Res.* 107:8046. doi: 10.1029/2000JC000583

Eicken, H., Reimnitz, E., Alexandrov, V., Martin, T., Kassens, H., and Viehoff, T. (1997). Sea-ice processes in the Laptev Sea and their importance for sediment export. *Cont. Shelf Res.* 17, 205–233. doi: 10.1016/s0278-4343(96)00024-6

Fowler, S. W. (2011). ^{210}Po in the marine environment with emphasis on its behavior within the biosphere. *J. Environ. Radioact.* 102, 448–461. doi: 10.1016/j.jenvrad.2010.10.008

Grenier, M., Francois, R., Soon, M., van der Loeff, M. R., Yu, X., Valk, O., et al. (2019). Changes in circulation and particle scavenging in the Amerasian Basin of the Arctic Ocean over the last three decades inferred from the water column distribution of geochemical tracers. *J. Geophys. Res.* 124, 9338–9363. doi: 10.1029/2019jc015265

Hebbeln, D., and Weber, G. (1991). Effects of ice coverage and ice-rafted material on sedimentation in the fram strait. *Nature* 350, 409–411. doi: 10.1038/350409a0

Jweda, J., and Baskaran, M. (2011). Interconnected riverine-lacustrine systems as sedimentary repositories: A case study in southeast Michigan using excess ^{210}Pb- and ^{137}Cs-based sediment accumulation and mixing models. *J. Great Lakes Res.* 37, 432–446. doi: 10.1016/j.jglr.2011.04.010

Kadko, D., and Landing, W. M. (2015). *U.S. Arctic GEOTRACES Cruise Report*. Available Online at: https://www.bodc.ac.uk/resources/inventories/cruise_inventory/reports/healy1502.pdf

Kim, G., Hong, Y.-L., Jang, J., Lee, I., Hwang, D.-W., and Yang, H.-S. (2005). Evidence for anthropogenic ^{210}Po in urban atmosphere of Seoul, Korea. *Environ. Sci. Technol.* 39, 1519–1522. doi: 10.1021/es049023u

Kim, G., Hussain, N., and Church, T. M. (2000). Excess ^{210}Po in the coastal atmosphere. *Tellus B* 52, 74–80. doi: 10.1034/j.1600-0889.2000.00975.x

Kipp, L. E., Charette, M. A., Moore, W. S., Henderson, P. B., and Rigor, I. G. (2018). Increased fluxes of shelf-derived materials to the central Arctic Ocean. *Sci. Adv.* 4:eaao1302. doi: 10.1126/sciadv.aao1302

Krembs, C., Eicken, H., and Deming, J. W. (2011). Exopolymer alteration of physical properties of sea ice and implications for ice habitability and biogeochemistry in a warmer Arctic. *Proc. Natl. Acad. Sci.* 108, 3653–3658. doi: 10.1073/pnas.1100701108

Krupp, K. D. (2017). *Using ^{210}Po/^{210}Pb disequilibria to characterize the biogeochemistry and quantify the dynamics of sea ice in the Arctic. M.S. thesis*. Detroit: Wayne State University.

Landa, E. R., Reimnitz, E., Beals, D. M., Pochkowski, J. M., Winn, W. G., and Rigor, I. (1997). Transport of ^{137}Cs and ^{239,240}Pu with ice-rafted debris in the Arctic Ocean. *Arctic* 51, 27–39.

Marley, N. A., Gaffney, J. S., and Drayton, P. J. (2000). Measurement of ^{210}Pb, ^{210}Po and ^{210}Bi in size-fractionated atmospheric aerosols: an estimate of fine-aerosol residence times. *Aerosol. Sci. Technol.* 32, 569–583. doi: 10.1080/027868200303489

Marsay, C. M., Aguilar-Islas, A., Fitzsimmons, J. N., Hatta, M., Jensen, L. T., John, S. G., et al. (2018). Dissolved and particulate trace elements in late summer Arctic melt ponds. *Mar. Chem.* 204, 70–85. doi: 10.1016/j.marchem.2018.06.002

Morton, P. L., Landing, W. M., Hsu, S. C., Milne, A., Aguilar-Islas, A. M., Baker, A. R., et al. (2013). Methods for the sampling and analysis of marine aerosols: results from the 2008 GEOTRACES aerosol intercalibration experiment. *Limnol. Oceanogra. Methods* 11, 62–78. doi: 10.4319/lom.2013.11.62

Masqué, P., Cochran, J. K., Hirschberg, D. J., Dethleff, D., Hebbeln, D., Winkler, A., et al. (2007). Radionuclides in Arctic sea ice: Tracers of sources, fates, and ice transit time scales. *Deep-Sea Res. I* 54, 1289–1310. doi: 10.1016/j.dsr.2007.04.016

McNeary, D., and Baskaran, M. (2003). Depositional characteristics of ^{7}Be and ^{210}Pb in Southeastern Michigan. *J. Geophys. Res.* 108:D04210. doi: 10.1029/2002JD003021

McNeary, D., and Baskaran, M. (2007). Residence times and temporal variations of ^{210}Po in aerosols and precipitation from Southeastern Michigan, USA. *J. Geophys. Res.* 112:D04208. doi: 10.1029/2006JD007639

Meese, D. A., Reimitz, E., Tucker, W. B., Gow, A. J., Bischoff, J., and Darby, D. (1997). Evidence for radionuclide transport by sea ice. *Sci. Total Environ.* 202, 267–278. doi: 10.1016/s0048-9697(97)00121-6

Melling, M., and Riedel, D. A. (2003). *Ice draft and ice velocity data in the Beaufort Sea, 1990-2003, Versions. 1*. Boulder, Colorado: National Snow and Ice Data Center.

Moore, H. E., Poet, S. E., and Martell, E. A. (1973). ^{222}Rn, ^{210}Pb, ^{210}Bi, and ^{210}Po profiles and aerosol residence times versus altitude. *J. Geophys. Res.* 78, 7065–7075.

Moore, R. M., and Smith, J. N. (1986). Disequilibria between ^{226}Ra, ^{210}Pb and ^{210}Po in the Arctic Ocean and the implications for chemical modification of the Pacific water inflow. *Earth Planet. Sci. Lett.* 77, 285–292. doi: 10.1016/0012-821x(86)90140-8

Niedermiller, J., and Baskaran, M. (2019). Comparison of the scavenging intensity, remineralization and residence time of ^{210}Po and ^{210}Pb at key zones (biotic, sediment-water and hydrothermal) along the East Pacific GEOTRACES transect. *J. Environ. Radioact.* 198, 165–188. doi: 10.1016/j.jenvrad.2018.12.016

Nürnberg, D., Wollenburg, I., Dethleff, D., Eicken, H., Kassens, H., Letzig, T., et al. (1994). Sediments in Arctic sea ice – implications for entrainment, transport and release. *Mar. Geol.* 119, 185–214. doi: 10.1016/0025-3227(94)90181-3

Perovich, D. K., Grenfell, T. C., Richter-Menge, J. A., Light, B., Tucker, W. B. III, and Eicken, H. (2003). Thin and thinner: sea ice mass balance measurements during SHEBA. *J. Geophys. Res.* 108:8050.

Pfirman, S. L., Eicken, H., Bauch, D., and Weeks, W. F. (1995). The potential transport of pollutants by Arctic sea ice. *Sci. Total Environ.* 159, 129–146. doi: 10.1016/0048-9697(95)04174-y

Polashenski, C., Perovich, D., and Courville, Z. (2012). The mechanisms of sea ice melt pond formation and evolution. *J. Geophys. Res.* 117:C01001.

Reimnitz, E., Kempema, E. W., and Barnes, P. W. (1987). Anchor ice, seabed freezing, and sediment dynamics in shallow arctic seas. *J. Geophys. Res.* 92, 14671–14678. doi: 10.1029/jc092ic13p14671

Rigaud, S., Puigcorbe, V., Camara-Mor, P., Casacuberta, N., Roca-Marti, M., Garcia-Orellana, J., et al. (2013). A method assessment and recommendations for improving calculations and reducing uncertainties in the determination of ^{210}Po and ^{210}Pb activities in seawater. *Limnol. Oceanogr. Methods* 11, 561–571. doi: 10.4319/lom.2013.11.561

Robbins, J. A. (1978). "Geochemical and geophysical applications of radioactive lead," in *The Biogeochemistry of Lead in the Environment*, ed. J. O. Nriagu (Amsterdam: Elsevier/North-Holland Biomedical Press), 285–393.

Robbins, J. A., Murdock, A., and Oliver, B. G. (1990). Transport and storage of ^{137}Cs and ^{210}Pb in sediments of Lake St. *Clair. Can. J. Fish. Aquat. Sci.* 47, 572–587.

Roberts, K. A., Cochran, J. K., and Barnes, C. (1997). ^{210}Pb, ^{239,240}Pu in the Northeast Water Polynya, Greenland: Particle dynamics and sediment mixing rates. *J. Mar. Syst.* 10, 401–413. doi: 10.1016/s0924-7963(96)00061-9

Roca-Marti, M., Puigcorbe, V., Rutgers van der Loeff, M. M., Katlein, C., Fernandez-Mendez, M., Peeken, I., et al. (2016). Carbon export fluxes and export efficiency in the central Arctic during the record sea-ice minimum in 2012: a joint ^{234}Th/^{238}U and ^{210}Po/^{210}Pb study. *J. Geophys. Res.* 121, 5030–5049. doi: 10.1002/2016jc011816

Rutgers van der Loeff, M., Kipp, L., Charette, M. A., Moore, W. S., Black, E., Stimac, I., et al. (2018). Radium isotopes across the Arctic Ocean show time scales of wáter mass ventilation and increasing shelf inputs. *J. Geophys. Res.* 123, 4853–4873. doi: 10.1029/2018jc013888

Rutgers van der Loeff, M. M., and Geibert, W. (2008). "U/Th series nuclides as tracers of particle dynamics, scavenging and biogeochemical cycles in the ocean," in *U-Th Series radionuclides in aquatic systems*, eds S. Krishnaswami and J. K. Cochran (Amsterdam: Elsevier).

Smith, J. N., Moran, S. B., and Macdonald, R. W. (2003). Shelf-basin interactions in the Arctic Ocean based on ^{210}Pb and Ra isotope tracer distributions. *Deep-Sea Res. I* 50, 397–416. doi: 10.1016/s0967-0637(02)00166-8

Sturm, M., Holmgren, J., and Perovich, D. K. (2002). Winter snow cover on the sea ice of the Arctic Ocean at the Surface Heat Budget of the Arctic Ocean (SHEBA): Temporal evolution and spatial variability. *J. Geophys. Res.* 107:8047.

Su, C. C., and Huh, C. A. (2002). Atmospheric ^{210}Po anomaly as a precursor of volcanic eruptions. *Geophys. Res. Lett.* 29:1070. doi: 10.1029/2001GL013856

Turekian, K. K., Nozaki, Y., and Benninger, K. (1977). Geochemistry of atmospheric radon and radon products. *Ann. Rev. Earth Planetary Sci.* 5:227. doi: 10.1146/annurev.ea.05.050177.001303

Uttal, T., Curry, J. A., McPhee, M. G., Perovich, D. K., Moritz, R. E., Maslanik, J. A., et al. (2002). Surface heat budget of the Arctic Ocean. *Bull. Am. Meteo. Soc.* 83, 255–275.

Wang, J., Zhong, Q., Baskaran, M., and Du, J. Z. (2019). Investigations on the time-series partitioning of ^{210}Pb, ^{207}Bi and ^{210}Po between marine particles and solution under different salinity and pH conditions. *Chem. Geol.* 528:119275. doi: 10.1016/j.chemgeo.2019.119275

Wilkening, M. H., and Clements, W. E. (1975). Radon-222 from ocean surface. *J. Geophys. Res.* 80, 3828–3830. doi: 10.1029/jc080i027p03828

Yang, W., Guo, L., Chuang, C., Schumann, D., Ayranov, M., and Santschi, P. H. (2013). Adsorption characteristics of ^{210}Pb, ^{210}Po and ^{7}Be onto micro-particle surfaces and the effects of macromolecular organic compounds. *Geochim. Cosmochim. Acta* 107, 47–64. doi: 10.1016/j.gca.2012.12.039

Conflict of Interest: The authors declare that the research was conducted in the absence of any commercial or financial relationships that could be construed as a potential conflict of interest.

Publisher's Note: All claims expressed in this article are solely those of the authors and do not necessarily represent those of their affiliated organizations, or those of the publisher, the editors and the reviewers. Any product that may be evaluated in this article, or claim that may be made by its manufacturer, is not guaranteed or endorsed by the publisher.